# Synthesis of Novel Cage-Like Mesoporous Vanadosilicate and Its Efficient Performance for Oxidation Dehydrogenation of Propane

**Yong-Mei Liu,* Song-Hai Xie, Yong Cao,* He-Yong He, and Kang-Nian Fan**

*Department of Chemistry and Shanghai Key Laboratory of Molecular Catalysis and Innovative Materials, Fudan University, Shanghai 200433, People's Republic of China*

*Received: October 12, 2009; Revised Manuscript Received: February 17, 2010*

Ordered vanadosilicate mesoporous material with large (~15 nm), uniform, novel cage-like mesopores was synthesized under acidic aqueous conditions from tetraethyl orthosilicate in the presence of ammonia vanadiate, using $P_{123}$ with CTAB as cotemplate and TMB as a swelling agent. The catalysts were extensively characterized by a combination of different techniques ($N_2$ adsorption, small-angle X-ray scattering (SAXS), transmission electron microscope (TEM), UV Raman, and UV−vis spectra) in relation to their performance for oxidation dehydrogenation of propane. SAXS and TEM analysis showed that the as-synthesized vanadosilicate samples have a uniform, well-defined cage-like mesostructure. UV Raman and UV−vis spectra revealed that the vanadium species was isolated and presented as a highly dispersed state in the framework of the vanadosilicate samples. Significantly enhanced catalytic activity was observed for the vanadosilicate catalysts, as compared with the 1.0 V-SBA-15 prepared by conventional impregnation. The enhanced catalytic activity of the vanadosilicate catalyst was attributed to the beneficial presence of a larger amount of isolated and highly dispersed V-species, as well as the cage-like mesoporous structure.

## 1. Introduction

Ordered mesoporous materials have received enormous attention owing to their high surface areas, regular frameworks, and large pore sizes with narrow distribution, all of which lead to multiple potential applications.[1,2] It is generally accepted that mesoporous materials with 3D pore systems exhibit more advantages in mass diffusion and transportation compared with MCM-41 materials[3,4] containing 1D channel. Cubic mesoporous silicas MCM-48, SBA-1, and SBA-16 with 3D hexagonal structures have been synthesized;[3−6] most of these cubic and 3D hexagonal mesoporous materials have cage-like pore structures, in which relatively large cavities are connected by some pore entrances with smaller sizes. However, there is a significant disadvantage of cubic mesoporous silicas that there are few catalytically active sites on its amorphous $SiO_2$ wall. Incorporation of various heteroatoms, such as Al, Sn, Zn, Mn, Ti, Mo, and V, into mesoporous molecular sieves especially with cubic mesoporous material is of tremendous interest in order to embed a catalytic function.[7−13]

Vanadium-containing catalysts are used in a large number of heterogeneous catalytic reactions such as oxidative dehydrogenation of alkanes, oxidation of aromatic hydrocarbons, and selective catalytic reduction of nitrogen oxides.[14−17] Considerable research has been focused on the synthesis and characterization of V-substituted mesoporous silicas such as HMS, MCM-41, MCM-48, SBA-15, and MCF.[18−26] V-mesoporous silica such as V-HMS,[23] V-MCM-41/48,[24,25] V-SBA-15,[22] and V-MCF[26] exhibit high activity in ODH of propane. It has been widely accepted that structural, textural, and acid/base properties and the nature of V species (oxidation state, coordination sphere, dispersion, and stability) play important roles in the activity of mesoporous material in ODH. Isolated or polymeric tetrahedral $V^{5+}$ species, obtained by spreading the oxide onto a support, are the most selective for the oxidative dehydrogenation (ODH) to alkenes.[22−28] It has been recently reported that isolated tetrahedral vanadium species show the highest intrinsic activity for ODH.[26,29] As a result, great efforts have been directed to prepare highly dispersed isolated vanadium species on the support through using large surface area support or decreasing the vanadium loading. In the V-substituted mesoporous silica materials, it was found that the amount of vanadium atoms that can be incorporated into the MCM material structure by direct synthesis is limited,[30] leading to the segregation of excess vanadium as vanadia. However, it is more difficult to synthesize V-substituted mesoporous under high acidic conditions by direct synthesis.[31]

Herein, we report vanadium-substituted novel cage-like mesoporous silicas with large cavity (~15 nm) and large entrance size (~5 nm); the anionic V species favored the incorporation of V into the silica framework according to the $S^+X^-I^+$ synthesis route like the Mo-SBA-1 synthesis.[32,33] Cage-like vanadosilicate mesoporous molecular sieves were synthesized under acidic conditions, using $P_{123}$ with CTAB as cotemplate and 1,3,5-trimethylbenzene (TMB) as the organic swelling agent, tetraethyl orthosilicate [$Si(OC_2H_5)_4$, TEOS] as a silica source, and ammonium vanadate ($NH_4VO_3$) as a vanadium source. These novel cage-like mesoporous vanadosilicate materials showed much better performance in the oxidative dehydrogenation of propane than those vanadium oxides supported on conventional mesoporous silica such as SBA-15.

## 2. Experimental Section

**2.1. Preparation of Catalysts.** A typical synthesis was conducted as follows: Cetyltrimethylammonium bromide (CTAB), $P_{123}$, HCl (1.6 M), and distilled water were mixed to obtain a homogeneous solution at 40 °C, then 1,3,5-trimethylbenzene (TMB) was added and the mixture was stirred for another 2 h. TEOS and vanadium precursor solution ($NH_4VO_3$) were added

* To whom correspondence should be addressed. E-mail: yongcao@fudan.edu.cn and ymliu@fudan.edu.cn.

10.1021/jp909749w 
Published on Web 03/10/2010

to the above mixture with vigorous stirring. After being stirred for 24 h, the mixture was allowed to react at 100 °C under static conditions for 24 h. The mass ratio of the gel was as follows: $P_{123}$:CTAB:TMB:1.6MHCl:TEOS:$NH_4VO_3$ = 2:1:1:75:4.25:$n$ (0.022−0.22); and the samples was denoted as S$x$ ($x$ meaning the molar ratio of the Si/V of the starting gel). The precipitate was filtered after 24 h, dried at 120 °C overnight, and then calcined in air at 550 °C for 4 h. For comparison, vanadia catalyst supported on SBA-15 was prepared by impregnation as previously reported.[22]

**2.2. Catalyst Characterization.** Nitrogen adsorption and desorption at 77 K were measured using a Micromeritics Tristar 3000 after the samples were degassed ($1.33 \times 10^{-2}$ Pa) at 300 °C overnight. The specific surface area was calculated by using the BET method, and pore size distribution was determined by the BJH method.

Small-angle X-ray scattering (SAXS) experiments were performed on a German Bruker NanoSTAR U SAXS system equipped with a high-resolution pinhole chamber, using Cu Kα radiation ($\lambda$ = 1.518 Å) and a 106 cm sample-to-detector distance. Transmission electron microscope (TEM) images were recorded digitally with a Gatan slow-scan charge-coupled device camera on a JEOL 2011 electron microscope operating at 200 kV. The samples were prepared by dispersing the powder products as slurry in acetone, which was then deposited and dried on a holey carbon film on a Cu grid.

Diffuse reflectance UV−vis spectra were collected on a Varian Cary 5 spectrophotometer equipped with a "Praying Mantis" attachment from Harrick. The sample cell was equipped with a heater unit, a thermocouple, and a gas flow system for in situ measurements. The samples were dehydrated in situ in dry air at 550 °C for 4 h. The spectra were recorded after cooling to room temperature, with dry air flowed through the sample to avoid rehydration. The absorption edge energy values were determined from the energy intercept of a linear fit passing through the near-edge region in a plot of $[F(R_\infty)\cdot h\nu]^{1/2}$ vs $h\nu$, where the first parameter refers to the Kubelka−Munk function and $h\nu$ is energy of the incident photon.[26,34,35]

In situ laser Raman spectra were obtained with use of a confocal microprobe Jobin Yvon Lab Ram Infinity Raman system equipped with both visible and UV excitation lines. The UV Raman measurements were carried out using the UV line at 325 nm from a Kimmon IK3201R-F He−Cd laser as the exciting source, with a laser output of 30 mW and a maximum incident power at the sample of approximately 6 mW.

**2.3. Catalytic Tests.** The catalytic properties of the samples were investigated in a fixed-bed quartz tubular flow reactor (6 mm i.d., 400 mm long) equipped with several gas flow lines with mass flow controllers to supply the feed, consisting of a mixture of propane/oxygen/nitrogen with a molar ratio of 1/1/8. The temperature in the middle of the catalytic bed was measured with a coaxial thermocouple. Catalyst samples (60−80 mesh) were introduced into the reactor and diluted with 300 mg of quartz powder (40−60 mesh) to maintain a constant volume in the catalyst bed. The feed and the reaction products were analyzed online by a gas chromatograph (type GC-122, Shanghai). Permanent gases ($O_2$, CO, and $CO_2$) were separated with use of a TDX-01 column connected to a thermal conductivity detector, and other reaction products were analyzed by using a Porapak Q column connected to a flame ionization detector. Blank runs showed that under the experimental conditions used in this work, the homogeneous reaction could be neglected.

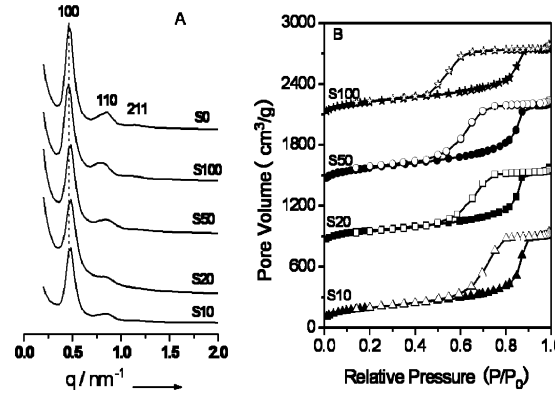


**Figure 1.** Small-angle X-ray scattering (SAXS) patterns of various vanadosilicate materials (A) and nitrogen sorption isotherms (B).

**TABLE 1: Physicochemical Properties of Calcined Vanadosilicate Mesoporous Samples**

| sample | Si/V ratio (in gel) | $V^b$ (wt %) | $a_0$ [nm] | BET surface area [m$^2$/g] | pore vol [cm$^3$/g] | pore size [nm]$^a$ | entrance size [nm]$^a$ | Si/V ratio [in product]$^b$ |
|---|---|---|---|---|---|---|---|---|
| S0 | | | 29.0 | 713 | 1.11 | 15.2 | 4.1 | |
| S100 | 100 | 0.13 | 29.0 | 697 | 1.26 | 14.8 | 5.2 | 664 |
| S50 | 50 | 0.32 | 30.3 | 739 | 1.28 | 14.8 | 5.3 | 264 |
| S20 | 20 | 0.76 | 29.0 | 805 | 1.31 | 14.7 | 5.4 | 110 |
| S10 | 10 | 0.90 | 29.0 | 819 | 1.25 | 15.1 | 5.5 | 93 |
| 1.0 V-SBA | | 0.94 | 11.2 | 592 | 1.09 | 7.1 | | |

$^a$ Calculated from the desorption branch of the $N_2$ adsorption/desorption isotherms based on the BJH model. Note that the as-estimated entrance size may be smaller in comparison to the value calculated based on the DFT model. $^b$ Determined by ICP.

## 3. Results and Discussion

**3.1. Structural Characteristics of Vanadium-Substituted Cage-Like Mesoporous Samples.** The vanadium-substituted cage-like mesoporous vanadosilicate samples were analyzed by using SAXS. X-ray scattering is observed if uniformly sized particles are present, as opposed to X-ray diffraction associated with periodic structures.[26,36] Figure 1A shows the recorded SAXS data for the vanadosilicate samples with different Si/V ratio. The patterns show three well-resolved peaks, which can be assigned to the {100}, {110}, {211} and reflections of a face-centered cubic structure. The unit cell parameters calculated from the SAXS data are in the range 29−31 nm (Table 1) for different samples. From the patterns, we find there are no shifts of the primary peak and no decrease of the intensity of {100} with increase in the vanadium content, suggesting the vanadosilicate samples retained the perfect face-centered cubic structure after the incorporation of vanadium, as can be seen from the TEM and $N_2$ adsorption data.

Normally, the conventional large pore cage-like mesoporous silica, such as SBA-16 or FDU-1, shows a large H1 hysteresis loop.[6] On the other hand, no hysteresis loop is observed in SBA-1 in which the sizes of cavities and entrances are relatively smaller. In our case, it is noteworthy that the hysteresis loops become slightly smaller with the vanadium content increase even as typical H1 hysteresis loops. Accordingly, the shift of desorption branches to high relative pressure indicates that the entrance size of the sample have been enlarged by incorporation of the vanadium. It is noteworthy that both the cavity and the entrance size distributions of vanadosilicate samples are quite narrow, as can be seen from the steep change from the adsorption and desorption branches. The sizes of the cavities and the entrances as well as other physical parameters of the samples are listed in Table 1. As given in Table 1, both the silicieous and V-incorporation samples exhibited reasonably high

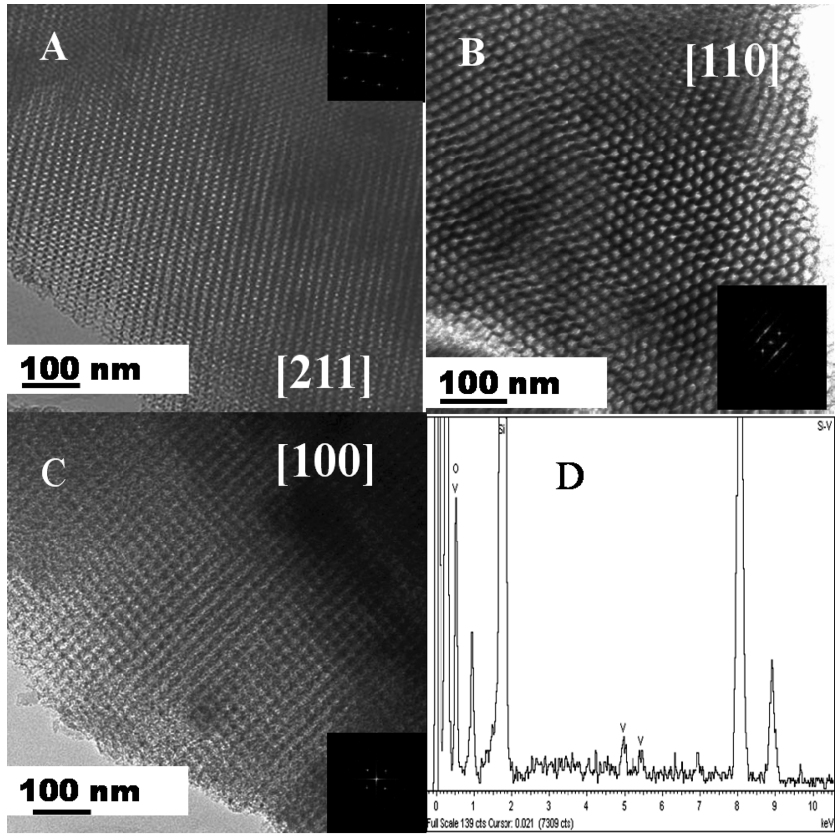


**Figure 2.** TEM images projected along the direction (A) [211], (B) [110], and (C) 100 of the calcined cage-like vanadosilicate S10 sample and EDS spectrum (D) of the S10 sample collected from the former region.

BET specific surface areas in the range 700−830 $m^2\ g^{-1}$. There is no decrease in the surface areas and pore volumes after the incorporation of vanadium into the samples, but a slight increase, suggesting the incorporation of vanadium makes no perturbation on the pore structure of the cage-like mesoporous, which is in agreement with the results of the SAXS results.

Transmission electron microscope (TEM) images and corresponding Fourier diffractograms recorded along the [211], [110], and [100] directions of S10 samples are shown in Figure 2. The highly ordered lattice array over large domains under the TEM observations suggests that the vanadosilicate products have a uniform, well-defined cage-like cubic mesostructure ($Fm\bar{3}m$).[1] Taken directly from the images, the unit cell parameter $a$ is estimated to be 31 nm, which is in good accordance with the XRD results. The diameter of the cages may be directly measured from the edge of the particle in Figure 2B to be about 15.2 nm, in good accordance with the $N_2$ sorption result (Figure 1B). And in our case, the diameter of the cage is larger than that of other cubic mesostructured pure silica materials.[1,3−6] The energy-dispersive X-ray (EDX) spectrum (an example is shown in Figure 2D) also shows evidence of the vanadium species in the framework of the cage-like vanadosilicate samples. The vanadium content of the samples determined by ICP is listed in Table 1. From Table 1 it is found that the ratio of the Si/V in the products is smaller than the ratio in the gel, but the ratio in the product is comparable with those reported for vanadium mesoporous materials by direct hydrothermal methods.[37]

**3.2. Chemical States of the V Species.** We have studied the nature and environment of the V species in the vanadosilicate samples by diffuse reflectance UV−visible spectroscopy. This technique allows distinguishing both tetrahedral and octahedral V species. The selected UV−visible spectra of these samples are presented in Figure 3. The diffuse reflectance UV−visible

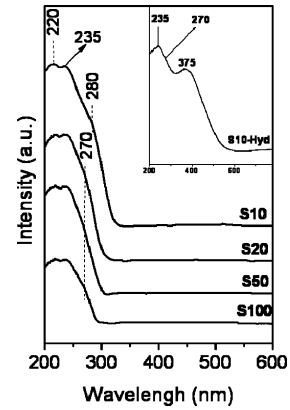


**Figure 3.** Diffuse reflectance UV−vis spectra of various vanadosilicate materials.

spectra of calcined and dehydrated samples exhibit two bands at around 220, 235 nm and a shoulder at 270 nm (Figure 3). The band at 220 nm can be attributed to the charge transfer of terahedrally coordinated $V^{IV}$ as literature reported,[37] and the band at 235 nm and the shoulder at 270 nm suggest the presence of two different kinds of tetrahedral $V^{V}$, strongly and less distorted, respectively, in agreement with the results reported for the $KVOF_4$ compound and the $VO_4^{3-}$ complex.[38,39] The result suggested the incorporation of vanadium into the framework of vanadosilicate samples. The intensities of the bands at 270 nm increase with the amount of vanadium. It should be noted that the absence of typical bands at ∼330 and 480 nm of $V_2O_5$ in the spectrum of all the samples implies that no crystalline $V_2O_5$ was formed and the vanadium species was isolated and presented as a highly dispersed state in the framework of vanadosilicate samples.

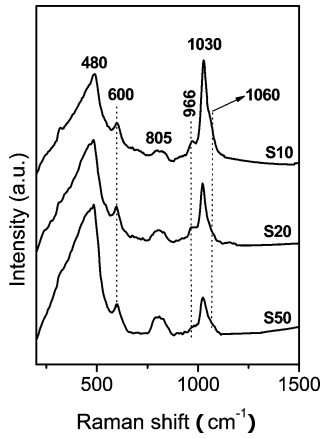


**Figure 4.** UV−Raman spectra of vanadosilicate catalysts excited by the 325-nm laser line.

The UV−visible spectrum of S10-Hyd with high V content shows the presence of two kinds of tetrahedral $V^V$. The first is identified by the band at 235 nm and the second one by the shoulder at about 270 nm, which is less distorted than that observed at 240 nm (inset to Figure 3). Moreover, the octahedral $V^V$ are identified by the band at 375 nm. This suggests that upon rehydration of the S10 sample, some of the more distorted tetrahedral V species are still present in the sample, but the major part, which is in a less distorted tetrahedral environment, is transformed into octahedral V species. The increase of the intensity and the constant position of the band at 375 nm as a function of time of exposure to moist air indicate that this band represents mononuclear $V^V$ in octahedral coordination. The high dispersion in the mesoporous structure of these species and their interaction with water molecules are confirmed by the disappearance of the band at 375 nm after removal of adsorbed water upon calcination. Furthermore, the large width of the band at 375 nm suggests that this band can be related to a mixture of different octahedral $V^V$ species. The UV−visible studies show that tetrahedral $V^V$ species in the S10 sample with higher V content can change their coordination in contact with moist air to square-pyramidal or octahedral. This suggests that when the V content increases, $V^V$ ions are incorporated in a site more accessible to water. The presence of well-dispersed mononuclear $V^V$ species in S10-Hyr is also supported by the fact that the color change between yellow and white is fully reversible upon calcination/rehydration cycles. Such a reversible behavior would be difficult for oligomeric $V^V$ species.[38]

Raman spectroscopy has been extensively used in the determination of structures of complex transition metal oxides. In contrast, the UV Raman spectroscopy has improved properties and can successfully avoid the surface fluorescence that often obscures the normal Raman spectra. Here the UV−Raman spectra of vanadosilicate samples with different vanadium content are shown in Figure 4. The measurements were performed at 200 °C in $N_2$ gas flow to keep the sample dehydrated since it was shown that the hydration of the vanadosilicate samples would greatly affect the Raman spectra.[22,26] As shown in Figure 4, the Raman bands at 480, 600, ∼805, 966, and 1030 with a weak shoulder at 1060 $cm^{-1}$ are observed for the vanadosilicate samples. The bands at 480 and 600 $cm^{-1}$ are assigned to D2 and D1 defect modes, which have been attributed to tri- and tetracyclosiloxane rings produced via the condensation of surface hydroxyls, respectively.[41−43] The broad bands at ∼805 $cm^{-1}$, which have been assigned to the symmetrical Si−O−Si stretching mode,[41,43] decrease with increasing vanadium content, suggesting the breaking of Si−O−Si bridges. And the band at 966 $cm^{-1}$ is possibly assigned to the surface silanol groups of sample similar to that of Li group's result observed in the V-MCM-41 system.[44]

The band at ca. 1030 $cm^{-1}$ has been assigned to the V═O stretching vibration of monometric vanadium species bound directly to the support.[44−47] The intensity of the $\nu$(V═O) band of monomeric species at 1030 $cm^{-1}$ increased with vanadia content. Therefore the shoulder at 1060 $cm^{-1}$ is reasonably assigned to a tetrahedral V═O group bonded to the silica host. It should be noted that the band position (1060 $cm^{-1}$) of vanadosilicate is higher than that of tetrahedral vanadate in the literature (ca. 1030 $cm^{-1}$).[46] An empirical relationship between V−O bond lengths and Raman stretching frequencies has been assumed based on vanadium oxides.[47] According to this assumption, a higher frequency position corresponds to shorter V−O bonds; the highest frequency position at 1060 $cm^{-1}$ thus corresponds to the shortest V═O bond distance.[44] This result provides evidence for the isolated mono-oxo vanadate species in vanadosilicate molecular sieve being of tetrahedral structure with strong structural tension. The absence of typical bands at 335 and 920 $cm^{-1}$ of the bending mode of the V−O−V bond and symmetric OVO stretching of the polymeric vanadia species, respectively,[26] implies that no crystalline $V_2O_5$ or polymeric vanadia species exists in the vanadosilicate samples. We previously proposed from UV−vis results the presence of two types of monomeric species on the dehydrated surface of our catalysts. These species corresponds to two types of $V^{5+}$ cations, one type with one V═O bond and three bridging V−O−Si bonds and another type with one V═O bond, two bridging V−O−Si bonds, and one V−OH group. As a result of the existence of two monomeric species, their $\nu$(V═O) band positions should be close, and this result is confirmed by the Raman result, there two $\nu$(V═O) bands can be distinguished in the Raman spectra of the dehydrated catalysts although one of them is very weak.

**3.3. Catalytic Studies.** The remarkable activity of the vanadosilicate catalyst can be seen from Table 2. No reaction occurred without catalyst under the reaction conditions used here. Propane was also converted over pure silica sample S0. The introduction of V remarkably increased propane conversion and the selectivity for partial oxidation products. Propene was formed with high selectivity over the vanadosilicate catalysts with higher V content and the propene yield was comparable with that obtained over V-SBA catalysts.[22] As shown in Table 2, all the vanadosilicate catalysts result in the formation of an appreciable amount of acrolein. Similar catalytic behavior has been observed over V catalysts supported on mesoporous silicas such as MCM-41, HMS, SBA-15, and MCF.[22−26] It should be noted that ethylene was produced in a substantial amount over vanadosilicate via oxidative cracking of propane but smaller than our previous result,[22] so that the cage-like vanadosilicate catalyst showed much higher proprene selectivity.[26] From the results of Table 2, it also can be seen that the CO and $CO_2$ selectivities increase with V content present a higher $CO/CO_2$ ratio, which is similar to that for the V-MCM-41.[25] CO is preferentially formed by deep oxidation of propene while $CO_2$ is mainly formed through deep oxidation of both propane and propene.[25] It is remarkable that propene selectivity of up to 63% at a high propane conversion of 34.2% could be achieved over the vanadosilicate (S10) catalyst, so the propene yield reached 21.6%.

It is also clear from Table 2 that the S10 exhibited much higher propane conversion and selectivity to propene than

**TABLE 2: Oxidative Dehydrogenation of Propane over Vanadosilicate Catalysts[a]**

| | | selectivity (%) | | | | | | | |
|---|---|---|---|---|---|---|---|---|---|
| sample | concn (%) | $C_3H_6$ | $C_2H_4$ | $C_3H_4O$ | CO | $CO_2$ | yield (%) | yield (sum)(%) | TOF × $10^{21}$/$\mu$mol-$C_3H_6$ at.-$V^{-1}$ $s^{-1}$ |
| S0 | 3.3 | 36.3 | | | 21.2 | 42.5 | 1.2 | 1.2 | |
| S100 | 12.6 | 79.1 | 5.4 | 3.7 | 4.6 | 6.6 | 10 | 10.7 | 130 |
| S50 | 21.0 | 70.0 | 10.6 | 5.3 | 8.6 | 3.8 | 14.7 | 16.7 | 82.5 |
| S20 | 31.1 | 64.0 | 12.9 | 6.7 | 13.5 | 4.5 | 19.9 | 23.9 | 50 |
| S10 | 34.2 | 63.0 | 13.4 | 6.9 | 11.6 | 3.1 | 21.6 | 26.2 | 46 |
| 1.0 V-SBA | 24.7 | 51.0 | 29.2 | 4.9 | 9.1 | 2.4 | 12.6 | 19.8 | 35 |

[a] Reaction conditions: temperature ~575 °C; reaction pressure ~1 atm; gas flow ~12.5 mL/min; $C_3H_8$:$O_2$:$N_2$ = 1:1:8. Very small amounts of $CH_4$ and $C_2H_6$ were also detected, but are not shown here.

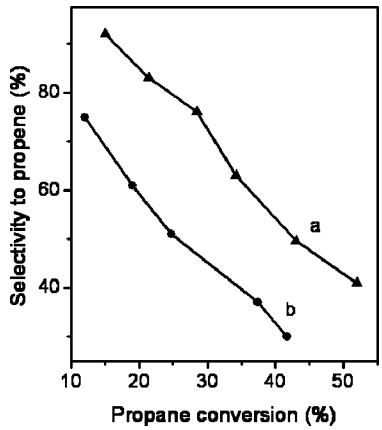


**Figure 5.** Variation of the selectivity to propylene with the propane conversion obtained during the oxidation of propane at 575 °C on different catalysts: (a) S10 vanadosilicate catalyst and (b) 1.0 V-SBA.

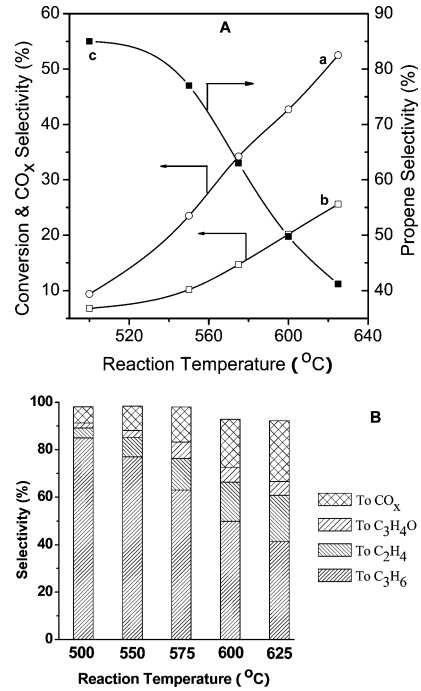


**Figure 6.** Influence of reaction temperature on the conversion of propane and product selectivity over vanadosilicate S10 catalyst.

mesoporous 1.0 V-SBA. Furthermore a higher ratio of CO to $CO_2$ was achieved over the 1.0 V-SBA sample. The high selectivity to propene on the former could be related to the monomeric V species on the large surface of the S10 sample with a large cage-like structure as described above, which is favorable for internal mass transfer.[26] Figure 5 compares the variation behavior of the selectivity to propene with the propane conversion on the vanadia dispersed on the two different siliceous supports at the same V loading level of ~1.0 wt %. It is seen that the selectivity to propene decreases with the propane conversion on the two samples. Moreover, it is observed that the vanadosilicate catalyst with a cage-like structure is more effective, as demonstrated by the higher activities and selectivity observed for this support, because its favorable, novel cage-like structure limits the consecutive reaction of propylene or allylic intermediates leading to deep oxidation.

The catalytic activity of the vanadosilicate catalysts was also found to be strongly dependent on the reaction temperature. The catalytic performance of the S10 catalyst at temperatures between 500 and 625 °C was investigated. Figure 6 plots the ODH of propane over the S10 catalyst as a function of reaction temperature. It was found that the S10 catalyst showed a poorer catalytic activity at a reaction temperature of 500 °C. The propane conversion increases rapidly with the increase in reaction temperature, especially below 600 °C. At 625 °C, the propane conversion reaches the highest value. It is noticeable that the change in behavior of the selectivity to $CO_x$ is the same trend of the conversion for propane over the temperature range investigated, which is completely different from the results obtained over V-SBA catalysts.[22] In comparison, the selectivity to propene showed the reverse behavior, but even at 625 °C the propene selectivity reached 42%, indicative of the highly selective nature of the S10 catalyst for the ODH of propane. It should also be noted that ethylene was obtained in substantial amounts over vanadosilicate via oxidative cracking of propane, but the ethane yield is relatively lower than that over V-SBA catalyst (table 2). It is remarkable that the propene yield exceeded 21% and propene selectivity of up to 63% at a high propane conversion of 34.2% could be achieved over the S10 vanadosilicate catalyst at 575 °C.

## 4. Conclusions

The present study demonstrates that a considerably large amount of V can be effectively incorporated into the novel cage-like mesoporous vanadosilicate under strongly acidic conditions. The vanadosilicate synthesized by direct synthesis method exhibits higher activity and selectivity for ODH of propane than the V-impregnated siliceous SBA-15 (V/SBA-15) catalysts, due to the presence of high dispersion and isolation of V species in the vanadosilicate framework.

**Acknowledgment.** This work was supported by the National Natural Science Foundation of China (20633030, 20703011, 20721063, 20803012, and 20873026), the National Basic Research Program of China (2003CB615807), the National High Technology Research and Development Program of China (2006AA03Z336), and Science & Technology Commission of Shanghai Municipality (09ZR1402300, 08DZ2270500).

## References and Notes

(1) Fan, J.; Yu, C. Z.; Gao, F.; Lei, J.; Tian, B. Z.; Wang, L. M.; Luo, Q.; Tu, B.; Zhou, W. Z.; Zhao, D. Y. *Angew. Chem., Int. Ed.* **2003**, *42*, 3146–3150.

(2) Davis, M. E. *Nature* **2002**, *417*, 813–821.

(3) Kresge, C. T.; Leonowicz, M. E.; Roth, W. J.; Vartuli, J. C.; Beck, J. S. *Nature* **1992**, *359*, 710–712.

(4) Beck, J. S.; Vartuli, J. C.; Roth, W. J.; Leonowicz, M. E.; Kresge, C. T.; Schmitt, K. D.; Chu, C. T. W.; Olson, D. H.; Sheppard, E. W. *J. Am. Chem. Soc.* **1992**, *114*, 10834–10843.

(5) Huo, Q. S.; Margolese, D. I.; Stucky, G. D. *Chem. Mater.* **1996**, *8*, 1147–1160.

(6) Zhao, D.; Huo, Q.; Feng, J.; Chmelka, B. F.; Stucky, G. D. *J. Am. Chem. Soc.* **1998**, *120*, 6024–6036.

(7) Grudzien, R. M.; Jaroniec, M. *Chem. Commun.* **2005**, 1076–1078.

(8) Hess, C.; Hoefelmeyer, J. D.; Tilley, T. D. *J. Phys. Chem. B* **2004**, *108*, 9703–9709.

(9) Hartmann, M.; Vinu, A.; Elangovan, S. P.; Murugesan, V.; Böhlmann, W. *Chem. Commun.* **2002**, 1238–1239.

(10) Vinu, A.; Dědeček, J.; Murugesan, V.; Hartmann, M. *Chem. Mater.* **2002**, *14*, 2433–2435.

(11) Che, S.; Sakamoto, Y.; Yoshitake, H.; Terasaki, O.; Tatsumi, T. *J. Phys. Chem. B* **2001**, *105*, 10565–10572.

(12) Shah, A. T.; Li, B. S.; Eldin, Z.; Abdalla, A. *J. Colloid Interface Sci.* **2009**, *336*, 707–711.

(13) Jermy, B. R.; Kim, S. Y.; Bineesh, K. V.; Selvaraj, M.; Park, D. W. *Microporous Mesoporous Mater.* **2009**, *121*, 103–113.

(14) Bulushev, D. A.; Kiwi-Minsker, L.; Zaikovskii, V. I.; Renken, A. *J. Catal.* **2000**, *193*, 145–153.

(15) Fierro, J. L. G.; Arrua, L. A.; Lopez Nieto, J. M.; Kremenic, G. *Appl. Catal., A* **1988**, *37*, 323–338.

(16) Roussel, H.; Mehlomakulu, B.; Belhadj, F.; van Steen, E.; Millet, J. M. M. *J. Catal.* **2002**, *205*, 97–106.

(17) Georgiadou, I.; Papadopoulou, C.; Matralis, H. K.; Voyiatzis, G. A.; Lycourghiotis, A.; Kordulis, Ch. *J. Phys. Chem. B* **1998**, *102*, 8459–8468.

(18) Berndt, H.; Martin, A.; Brückner, A.; Schreier, E.; Müller, D.; Kosslick, H.; Wolf, G.-U.; Lücke, B. *J. Catal.* **2000**, *191*, 384–400.

(19) Wei, D.; Wang, H.; Feng, X.; Chueh, W.-T.; Ravikovitch, P.; Lyubovsky, M.; Li, C.; Takeguchi, T.; Haller, G. L. *J. Phys. Chem. B* **1999**, *103*, 2113–2121.

(20) Mathieu, M.; Van Der Voort, P.; Weckhuysen, B. M.; Rao, R. R.; Catana, G.; Schoonheydt, R. A.; Vansant, E. F. *J. Phys. Chem. B* **2001**, *105*, 3393–3399.

(21) Van Der Voort, P.; Morey, M.; Stucky, G. D.; Mathieu, M.; Vansant, E. F. *J. Phys. Chem. B* **1998**, *102*, 585–590.

(22) Liu, Y. M.; Cao, Y.; Yi, N.; Feng, W. L.; Dai, W. L.; Yan, S. R.; He, H. Y.; Fan, K. N. *J. Catal.* **2004**, *224*, 417–428.

(23) Zhou, R.; Cao, Y.; Yan, S. R.; Deng, J. F.; Liao, Y. Y.; Hong, B. F. *Catal. Lett.* **2001**, *75*, 107–112.

(24) Solsona, B.; Blasco, T.; López Nieto, J. M.; Peña, M. L.; Rey, F.; Vidal-Moya, A. *J. Catal.* **2001**, *203*, 443–452.

(25) Peña, M. L.; Dejoz, A.; Fornés, V.; Rey, F.; Vázquez, M. I.; López Nieto, J. M. *Appl. Catal., A* **2001**, *209*, 155–164.

(26) Liu, Y. M.; Feng, W. L.; Li, T. C.; He, H. Y.; Dai, W. L.; Huang, W.; Cao, Y.; Fan, K. N. *J. Catal.* **2006**, *239*, 125–136.

(27) Owens, L.; Kung, H. H. *J. Catal.* **1993**, *144*, 202–213.

(28) LeBars, J.; Védrine, J. C.; Auroux, A.; Trautmann, S.; Baerns, M. *Appl. Catal., A* **1992**, *88*, 179–195.

(29) Pérez Pujol, A.; Valenzuela, R. X.; Fuerte, A.; Wloch, E.; Kubacka, A.; Olejniczak, Z.; Sulikowski, B.; Cortés Corberán, V. *Catal. Today* **2003**, *78*, 247–256.

(30) Gucbilmez, Y.; Dogu, T.; Balci, S. *Catal. Today* **2005**, *100*, 473–477.

(31) Schüth, F. *Chem. Mater.* **2001**, *13*, 3184–3195.

(32) Dai, L. X.; Teng, Y. H.; Tabata, K.; Suzuki, E.; Tatsumi, T. *Chem. Lett.* **2000**, *29*, 794–795.

(33) Huo, Q.; Margolese, D. I.; Stucky, G. D. *Chem. Mater.* **1996**, *8*, 1147–1160.

(34) Khodakov, A.; Yang, J.; Su, S.; Iglesia, E.; Bell, A. T. *J. Catal.* **1998**, *177*, 343–351.

(35) Khodakov, A.; Olthof, B.; Bell, A. T.; Iglesia, E. *J. Catal.* **1999**, *181*, 205–216.

(36) Schmidt-Winkel, P.; Lukens, W. W., Jr.; Yang, P.; Margolese, D. I.; Lettow, J. S.; Ying, J. Y.; Stucky, G. D. *Chem. Mater.* **2000**, *12*, 686–696.

(37) Dai, L. X.; Tabata, K.; Suzuki, E.; Tatsumi, T. *Chem. Mater.* **2001**, *13*, 208–212.

(38) Dzwigaj, S.; Matsuoka, M.; Anpo, M.; Che, M. *J. Phys. Chem. B* **2000**, *104*, 6012–6020.

(39) Hazenkamp, M. F.; Strijbosch, A. W. P. M.; Blasse, G. *J. Solid State Chem.* **1992**, *97*, 115–123.

(40) Ronde, H.; Snijders, J. G. *Chem. Phys. Lett.* **1977**, *50*, 282–283.

(41) Gao, X. T.; Bare, S. R.; Weckhuysen, B. M.; Wachs, I. E. *J. Phys. Chem. B* **1998**, *102*, 10842–10852.

(42) Morrow, B. A.; Mcfarlan, A. J. *J. Non-Cryst. Solids* **1990**, *120*, 61–71.

(43) Brinker, C. J.; Kirkpatrick, R. J.; Tallant, D. R.; Bunker, B. C.; Montez, B. *J. Non-Cryst. Solids* **1988**, *99*, 418–428.

(44) Xiong, G.; Li, C.; Li, H. Y.; Xin, Q.; Feng, Z. C. *Chem. Commun.* **2000**, *8*, 677–678.

(45) Chao, K. J.; Wu, C. N.; Chang, H.; Lee, L. J.; Hu, S. F. *J. Phys. Chem. B* **1997**, *101*, 6341–6349.

(46) Luan, Zh.; Meloni, P. A.; Czernuszewicz, R. S.; Kevan, L. *J. Phys. Chem. B* **1997**, *101*, 9046–9051.

(47) Hardcastle, F. D.; Wachs, I. E. *J. Phys. Chem.* **1991**, *95*, 5031–5041.

JP909749W